

Experimentally validated pre-design maps and performance estimation methods for small-scale turbopumps for organic Rankine cycles

Special issue paper

Article history:

Submission date: 28 March 2024

Final revision date: 23 September 2024

Acceptance date: 29 October 2024

Publication date: 22 May 2025



*Correspondence:

SZ: sajjad.zakeralhoseini@epfl.ch

Peer review:

Single blind

Copyright:

© 2025 Zakeralhoseini and Schiffmann @ This is an open access article distributed under the Creative Commons Attribution Non Commercial License (CC BY-NC 4.0), which permits unrestricted use, distribution, and reproduction in any medium for noncommercial purposes only, provided the original work is properly cited and its authors credited.

Keywords:

small-scale turbopump; organic Rankine cycle; computational fluid dynamics; experimental investigation; pre-design diagrams; 1D models

Citation:

Zakeralhoseini S. and Schiffmann J. (2025). Experimentally validated pre-design maps and performance estimation methods for small-scale turbopumps for organic Rankine cycles. *Journal of the Global Power and Propulsion Society*. 9: 17–32. <https://doi.org/10.33737/jgpps/195408>

Sajjad Zakeralhoseini^{1,*}, Jürg Schiffmann¹

¹Ecole Polytechnique Fédérale de Lausanne (EPFL), Laboratory for Applied Mechanical Design CH-1015 Lausanne, Switzerland

Abstract

The organic Rankine cycle (ORC) system is considered a promising technology to exploit thermodynamic potential of waste heat. Small-scale ORC applications, including both vehicular applications and stationary power plants, would greatly benefit from more compact and efficient pumps, improving performance and reducing installation and operational costs. This paper provides updated pre-design diagrams and reduced-order models that incorporate the effects of tip clearance and splitter blades in small-scale high-speed turbopumps for ORC applications. A parameterized design tool has been developed to enable the rapid generation of numerous turbopump geometries. The design tool creates a dataset of numerous turbopumps with different geometrical parameters. The turbopumps are investigated with CFD analysis, and the accomplished results are analyzed to characterize the influence of tip clearance and splitter blades on the performance (slip factor and head rise) of small-scale ORC turbopumps. The numerical results are employed to infer dimensionless maps (specific speed-specific diameter) and reduced-order models, which enable the capturing of the influence of down-scaling in the early design process of such machines. In the next step, two turbopumps are designed using the new design tool and then tested experimentally to validate the numerical model. The good agreement between experimental performance characteristics and developed models validates the computational results and reduced-order models. Following the experimental validation, the performance of an ORC system designed for waste heat recovery from truck engines is estimated using the performance characteristics of the experimental turbopumps instead of a commercial multi-stage centrifugal pump. The designed small-scale turbopumps are one order of magnitude more compact compared to commercial systems. Further, the comparison suggests that the designed turbopumps improve the targeted ORC thermal efficiency by 0.51% and reduce the ratio of the turbine power consumed by the pump by 42% and 67%.

Introduction

The organic Rankine cycle (ORC) is a thermodynamic process that shows exceptional features for exploiting waste heat sources across a wide range of temperatures (Wang et al. 2013a, b). This can be achieved by carefully selecting the working fluid, which allows for more efficient exploitation of low-grade waste heat (Yamamoto et al., 2001). Rijpkema et al. (2017) suggested that ORCs outperform other thermodynamic cycles regarding thermal efficiency. In the context of waste heat recovery

(WHR), [Lecompte et al. \(2015\)](#) identified the ORC as the most suitable solution for low-temperature sources (<350°C), a finding that was experimentally validated by [Benato and Macor \(2017\)](#).

As an example, ORCs have been used to recover waste heat from internal combustion engines on vehicles to increase the overall efficiency and reduce emissions. A 1.2–3.7% increase in engine efficiency was reported by [Galindo et al. \(2015\)](#) by using an ORC WHR system. Similarly, BMW ([Freyman et al. 2008](#); [Ringler et al. 2009](#)), Honda ([Ibaraki et al., 2007](#)), and Cummins ([Nelson, 2006](#)) proposed efficient ORC installations in passenger vehicles and trucks.

Typical organic fluids have lower latent heat than water, necessitating a higher mass flow rate to achieve equivalent power levels ([Bao and Zhao, 2013](#)). This significantly increases the size and power consumption of the pumping stage compared to systems designed for water ([Meng et al., 2017](#)). Consequently, the size of the pump and its efficiency play an increasingly important role in ORC compared to Rankine cycles. In particular, for small-scale ORC (<100 kWel), there is disagreement on the ideal pumping technology for ORC systems and a lack of investigation on small-scale pumps suitable for mobile ORC systems ([Yang et al. 2018a](#)).

Different types of commercial pumps were studied for ORC systems, such as multi-stage centrifugal pumps ([Meng et al., 2017](#); [Yang et al., 2019](#)), reciprocating pumps ([Landelle et al., 2017](#)), sliding vane pumps ([Bianchi et al., 2017](#)), Roto-Jet pumps ([Lei et al., 2016](#)), and diaphragm pumps ([Xu et al., 2017](#)). Previous research suggests that the choice of pump affects the ORC efficiency and that some pumps are more suitable for certain conditions than others. For instance, [Yang et al. \(2019\)](#) suggested using pumps with very low specific speeds to achieve a higher thermal efficiency of the ORC system. Meanwhile, [Yang et al. \(2018b\)](#) recommended that the thermal efficiency of the ORC system studied by [Meng et al. \(2017\)](#) can be improved if a hydraulic diaphragm metering pump is employed instead of the original multi-stage pump.

[Rosset et al. \(2021\)](#) recently published data on a gas-bearing supported radial inflow turbine designed for an ORC used for WHR on truck engines. They used a commercially available low-speed centrifugal pump with 27 stages (GRUNDFOS CRNE 1–27) to perform their experimental investigation. The size was six times larger than that of the 8 kW turbine. This highlights the need for smaller, more efficient pumps to make compact, high-power-density ORC more accessible.

Recent work on small-scale turbopumps highlights the feasibility of single-stage designs for driving typical ORC applications ([Zakeralhoseini and Schiffmann, 2023a](#)), which is particularly promising for achieving very compact and efficient designs. These high-power density solutions offer promising concepts for installing waste heat recovery systems in various vehicle types and sizes ([Xu et al., 2019](#)). Additionally, the reduced material requirements result in cost savings.

The design of turbomachinery is characterized by the sequential engagement of increasingly complex models ([Japikse et al., 2006](#); [Gülich, 2010](#)). The design process usually starts with design maps to identify overall dimensions and rotor speed and ends with 3D numerical flow simulations to fine-tune the geometry. Pre-design diagrams (0D models) for turbopumps (i.e., [Balje, 1962, 1981](#)) allow the engineers to quickly select the rotational speed and impeller outlet diameter for a given set of operating conditions. These maps relate efficiency to specific speed (Equation 1), and specific diameter (Equation 2), and allow narrowing down the solution space at the beginning of the design process.

$$n_q = \frac{5.5397nQ^{1/2}}{(gH)^{3/4}} \quad (1)$$

$$d_s = d \frac{(gH)^{1/4}}{Q^{1/2}} \quad (2)$$

The maps proposed by [Balje \(1962\), \(1981\)](#) are based on experimental data from large-scale pumps and are only applicable to pumps operating at high Reynolds numbers (>10⁸). However, for small-scale turbopumps as required for small-scale ORC (<15 kWel), typical Reynolds numbers range from 10⁵ to 10⁶, and predictions of impeller outlet diameter for a given set of operating conditions using classical Balje maps may entail significant inaccuracies. This leads to erroneous starting points in the design process ([Zakeralhoseini and Schiffmann, 2024](#)).

In a second step, 1D models (e.g., [Japikse et al., 2006](#); [Gülich, 2010](#)) allow to refine additional geometrical parameters such as impeller inlet diameters, blade angles, and volute dimensions. 1D models are based on the turbomachinery Euler equation and empirical loss correlations commonly derived from experimental data. The advantage of 1D models is that they are computationally efficient and can be used to explore a vast variety of design alternatives quickly. However, the 1D models available in the literature (e.g., [Gülich, 2010](#)) are developed based on large-scale turbopumps. Consequently, the influence of down-scaling, which may lead to an imperfect

similarity between models and small-scale machines (when they do not perfectly match in terms of scaling, design, or operational parameters (Gulich, 2010)) due to variations in Reynolds number, tip clearance ratio, and relative surface roughness, remains unaddressed (Diehl et al., 2020).

Much has been investigated regarding the slip factor to identify the difference between the metal blade and the actual flow angles, as evidenced by Gulich (2010) and von Backström (2005). However, a slip factor model applicable to unshrouded turbopump impellers is still lacking, and the impact of critical factors, such as tip clearance and splitter blades, on performance indicators like head coefficient and efficiency, remains poorly understood. Recent works by Zakeralhoseini and Schiffmann (2022a), (2023b) suggest that the slip factor is highly affected by off-design conditions and that both the slip factor and head rise coefficient are influenced significantly by the splitter blade design.

As a summary, state-of-the-art pre-design maps (0D-models) and 1D-meanline models fall short of accurately characterizing small-scale unshrouded turbopumps. This misleads the design process in the initial phase and complexifies the design of compact turbopumps for typical small-scale ORC applications.

The objective is to address these limitations by presenting updated n_q-d_s diagrams with efficiency estimations (pre-design maps/0D models), and revised 1D models that account for the effects of tip clearance and splitter blades in small-scale high-speed turbopumps specifically designed for ORC applications.

These models are developed through extensive CFD calculations and can be used for the preliminary design and optimization of such pumps. Notably, this study goes beyond previous research by presenting novel pre-design maps (0D models) and integrating both 0D and 1D models with experimental studies. Two small-scale turbopumps are designed and tested for an 8 kW ORC (Rosset et al., 2021) to validate the application of these models, demonstrating their effectiveness in properly designing ORC turbopumps. These validated pre-design maps (0D models) and 1D models adapted to reduced scale can aid in the initial design of centrifugal pumps for ORC applications. The validated model and the deviations observed between model predictions and experimental measurements represent novel contributions not previously studied.

Numerical procedure

To establish novel pre-design tools and 1D models, a wide array of reliable training and validation data is required. Therefore, a parametric design tool, which can rapidly create a turbopump geometry, is developed and coupled with numerical 3D computations to generate training data on an extensive range of geometries. The methodology implemented for this work is summarized in Figure 1. The design tool creates a dataset of 2,500 turbopump geometries for inferring updated pre-design maps, 576 geometries for a tip clearance model, and 1,620 geometries for a splitter blade model within the ranges specified in Table 1. For each set of parameters in Table 1, the design tool generates a turbopump geometry by incorporating the equations given in Table 2 (Figure 1, step A).

Stepanoff (1957) and Pfeiderer (2013) proposed correlations for determining the number of blades. In practical applications, however, the number of blades typically ranges between 5 and 7, with a tendency to decrease as specific speed increases (Nourbakhsh, 2005). In this study, the turbopump geometries used for generating the

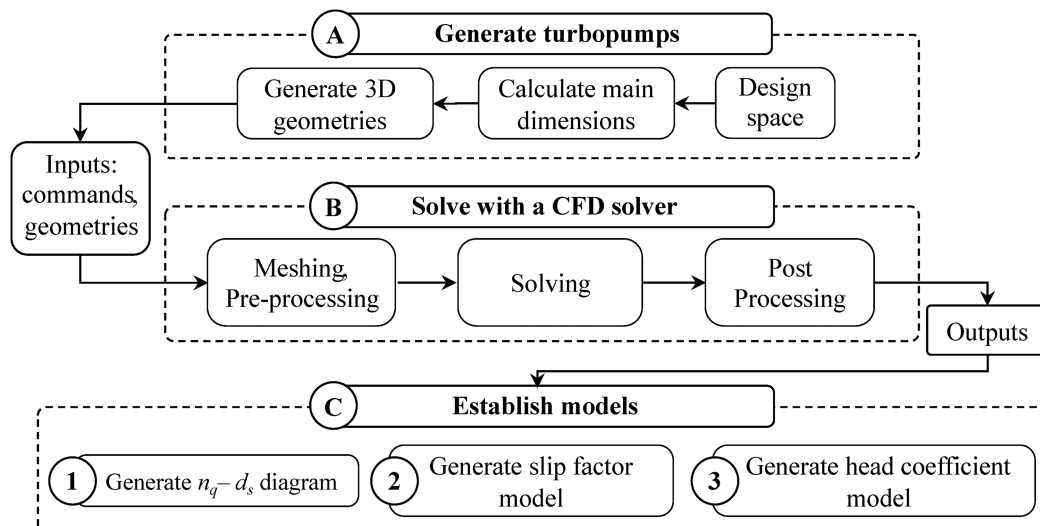


Figure 1. Data-driven methodology flowchart.

Table 1. Parameter ranges of turbopumps for CFD computations to infer updated Pre-design maps (0D-model), and tip-clearance and splitter blade loss correlations for the 1D-model.

Model	Parameter	Symbol	Unit	Range
Pre-design map	Rotational speed	n	krpm	15–100
	Mass flow rate	\dot{m}	kg/s	0.1–0.4
	Pressure rise	Δp	bar	10–25
	Blade outlet angle	β_{2B}	°	18–90
1D model: tip clearance	Blade outlet angle	β_{2B}	°	15, 22.5, 27.5, 32, 50, 90
	No. of blades	Z	–	5, 6, 7
	Tip ratio	c/b	–	0.05, 0.1, 0.15, 0.2, 0.3, 0.4, 0.6
	Rotational speed	n	krpm	40, 50, 63.5, 75
1D model: splitter blade	Blade outlet angle	β_B	°	22.5, 50, 90
	No. blades	Z	–	4, 5, 6
	Tip clearance ratio	c/b	%	shrouded, 0.05, 0.1
	Rotational speed	n	krpm	40, 50, 75
	Pitch of splitters	φ_{sp}	%	25, 37, 50, 62, 75
	Meridional location	$m'_{le,sp}$	%	25, 37, 50, 62

Table 2. Impeller equations.

Parameter	Equation	
Head coefficient (Gülich, 2010)	$\psi = 1.21 e^{-7.71266 \times 10^{-3} n_q}$	(3)
Impeller outlet diameter	$d_2 = 60/\pi n \sqrt{2gH/\psi}$	(4)
Inlet diameter	$d_{1,s} = 2.9 \left(\frac{Q_{imp}}{n(1-v^2) \tan \beta_{1d}} \times \left(1 + \frac{\tan \beta_{1d}}{\tan \alpha_1} \right) \right)^{1/3}$	(5)
Flow angle at the inlet	$\tan \beta_{1d} = (1-v^2)^{1.1} (125/n_{ss})^{2.2} (n_q/27)^{0.418}$	(6)
Leading edge angle	$\beta_{1B} = 0.975 \tan^{-1} \beta_1$	(7)
Inlet width	$b_1 = (1-v)d_1$	(8)
Outlet width	$b_2 = \left[0.017 + 2.62 \left(\frac{n_q}{1000} \right) - 8 \left(\frac{n_q}{1000} \right)^2 + 9.3 \left(\frac{n_q}{1000} \right)^3 \right] d_2$	(9)
Pitch of splitter blades	$\varphi_{sp} = \theta_{sp}/\theta_{mb}$	(10)
Meridional location of splitters	$m'_{le,sp} = m_{le,sp}/m_{mb}$	(11)
Slip factor	$\gamma = 1 - (C_{u2\infty} - C_{u2})/u_2$	(12)

data through CFD computations are designed with 5 to 7 blades. The pitch of the splitter blades, calculated with (Equation 10), determines their angular position within the main blade channel (see Figure 2). The relative position of the leading edge of the splitter blades ($m'_{le,sp}$) is determined by dividing the meridional location of the splitter blades' leading edge ($m_{le,sp}$) by the total meridional length of the main blade (m_{mb}).

Turbopump geometry generator and numerical methods

The automated turbopump geometry generation starts by establishing the main parameters of the impeller, followed by the design of a volute to collect the flow discharged from the impeller.

Impeller

The equations determining the impellers' parameters are summarized in Table 2. A hub ratio (ν) of 0.35 and a suction-specific speed (n_{ss}) of 220 are considered to size the inlet diameter. The meridional profiles are shaped systematically for a given medial axis and have a linear distribution of the impeller cross-section areas according to Zakeralhoseini and Schiffmann (2021). The coordinates of the medial axis (see Figure 2) are determined using a statistical model described in Zakeralhoseini and Schiffmann (2022a). The blade is shaped 3D and elliptically at the leading edge and narrows to a 2D shape at the trailing edge. The blade angles are determined by two parabolic curves that meet at a common tangent and have the same length, satisfying $\beta_{le} = \beta_{1B}$ and $\beta_{te} = \beta_{2B}$. The splitter blades are constructed by rotating the main blades along the axis of rotation and trimming their leading edge at a specific meridional length. Thus, the blade angle and thickness of the splitters match those of the main blades at every radius (see Figure 2). The slip factor is defined in (Equation 12), where $c_{u2\infty}$ denotes the circumferential component of absolute velocity for an impeller that hypothetically has an infinite number of blades. The slip factor adjusts the flow velocity at the impeller outlet and can be estimated using correlations available in the literature (e.g., von Backström, 2005; Gülich, 2010).

Volute

The width of the volute is the same as the impeller outlet width, and the cutwater is positioned at a 17° circumferential angle in the impeller rotation direction. The volutes are designed with elliptical or circular cross-sections, and the throat area follows the recommendations of Gülich (2010). To establish the volute cross-sections, the method of conservation of angular momentum (Pfleiderer, 2013) is used. A script is developed to create the 3D geometry of the volute and outlet pipe, utilizing the ANSYS Design Modeler (Release 2021 R1) engine to loft the volute profiles.

On average, the time required for generating each geometry is 6.3 s. Once a turbopump geometry is generated, the design tool initiates the CFD solver (Figure 1, step B). The solver is then given a set of appropriate commands to solve the flow passing through the pump. The analysis is conducted with ANSYS CFX 2021 R1.

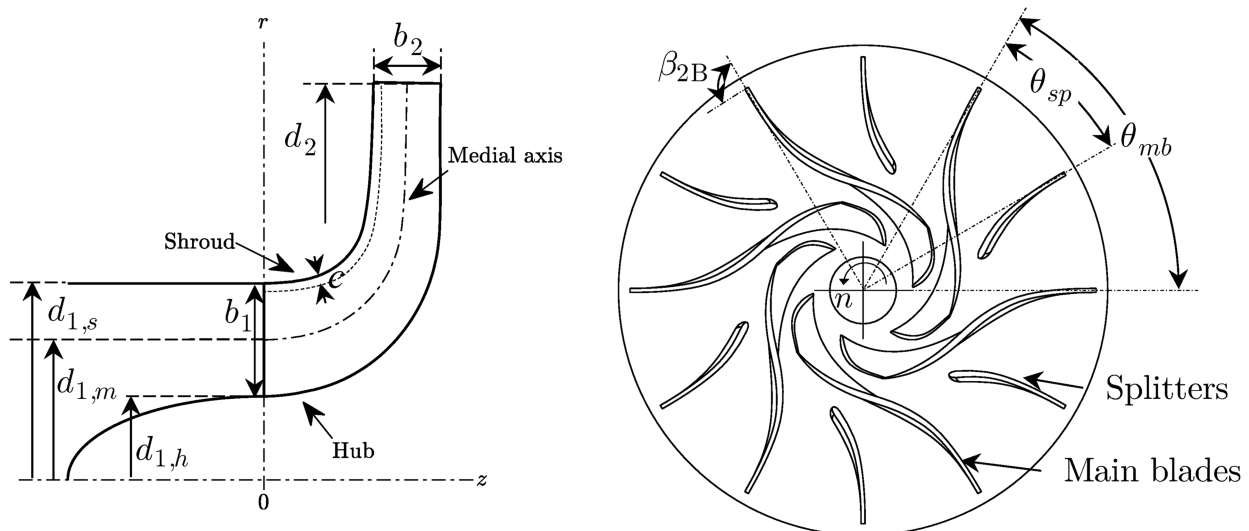


Figure 2. Impeller parameters and meridional curves.

CFD analysis

The impeller and inlet pipe are meshed using a structured grid, while the volute is meshed using an unstructured grid. The impeller grid is generated via ANSYS Turbogrid, utilizing J-Grid and O-Grid topologies, with grid sizes varying from 800,000 to 1,500,000 elements depending on the specific geometry. The volute mesh is generated with ANSYS Meshing to conserve its intricate geometry. The mesh comprises 1,500,000–10,000,000 elements for the diffuser and volute. A skewness of less than 0.3 is imposed for all geometries to ensure good mesh quality. The near-wall elements are adjusted to ensure y^+ values within the turbulence model validity range. A dense mesh comprising over 45 layers is employed for the tip clearance gap, with an end ratio ranging from 30 to 43.

The impeller is set as a relative flow domain, rotating at the pump speed. Steady-state simulations are performed assuming that the working fluid is R245fa in liquid state, using properties derived from REFPROP (Lemmon et al., 2018) at a temperature of 35°C and pressure of 4 bar, where the fluid exhibits a density of 1,311.6 kg/m³ and a dynamic viscosity of 352 μPa·s. The boundary conditions of total pressure and mass flow rate are set for the inlet pipe and volute discharge, respectively. The SST model (Menter et al., 2003) is used to model turbulence. The turbulence equations and advection term are discretized with a high-resolution scheme. Although the parameters of interest in this research—namely head rise, efficiency, and outlet flow conditions—typically converge within 150 iterations, a minimum of 400 iterations and an RMS residual target of 10⁻⁵ are established as convergence criteria. The computations are performed using six workstations, each equipped with Intel Xeon Processor E5-1650 v3 running at 3.50 GHz.

Post-processing is performed using ANSYS CFD-Post. The velocity variables (\bar{c} , \bar{w} , α and β) are computed as surface-weighted averages across cross-sectional planes. Total pressure (p_t) is calculated as the mass-weighted average. Data on velocity variables, pressures, and heads are collected at the pump inlet, impeller inlet, impeller outlet, and pump outlet. This allows for the calculation of key performance parameters, including the slip factor (Equation 12), pump head rise (Equation 13), and efficiency (Equation 14):

$$H = \frac{p_o - p_{in}}{\rho g} \quad (13)$$

$$\eta_t = 100 \times \frac{(p_o - p_{in})Q}{\dot{W}_{shaft}} \quad (14)$$

Pre-design maps and 1D models

The CFD results are then used to infer pre-design maps based on 2,500 geometries and 1D models considering the effects of tip clearance, using 576 geometries, and splitter blades, using 1,620 geometries, as shown in Figure 1, step C.

Pre-design maps

The non-dimensional parameters of specific speeds (n_q), specific diameters (d_s) and internal efficiency (η_i) are calculated and plotted on Cordier diagrams providing updated pre-design maps for the preliminary sizing of turbopumps suitable for small-scale ORC applications. Figure 3 presents the obtained n_q - d_s diagram for shrouded and unshrouded turbopumps with a 5% tip clearance ratio. The figure suggests that the feasible design region becomes narrower with decreasing specific speeds, as observed in the original Balje (1962) diagrams. Centrifugal pumps with a low specific speed suffer from high leakage losses, disk friction, and secondary flows (Olimstad et al., 2018), leading to a narrower range of feasible designs at low specific speeds. The figure suggests that the internal efficiency decreases with the increase of the specific diameter for a given specific speed, leading to a pattern of efficiency variations with the changes of n_q and d_s . The efficiency contours are plotted using interpolation on the original performance data to generate gridded n_q and d_s data. The contours suggest that unshrouded pumps with a 5% tip clearance ratio may invoke a significant efficiency drop (up to 56% relative) compared to shrouded machines.

Regression models for shrouded (Equation 15) and unshrouded pumps (Equation 17) were developed to predict the pump efficiency as a function of n_q and d_s based on the contour lines. Equations 16 and 18 can be used to estimate the ideal impeller outlet diameter, leading to the maximum efficiency (Table 3).

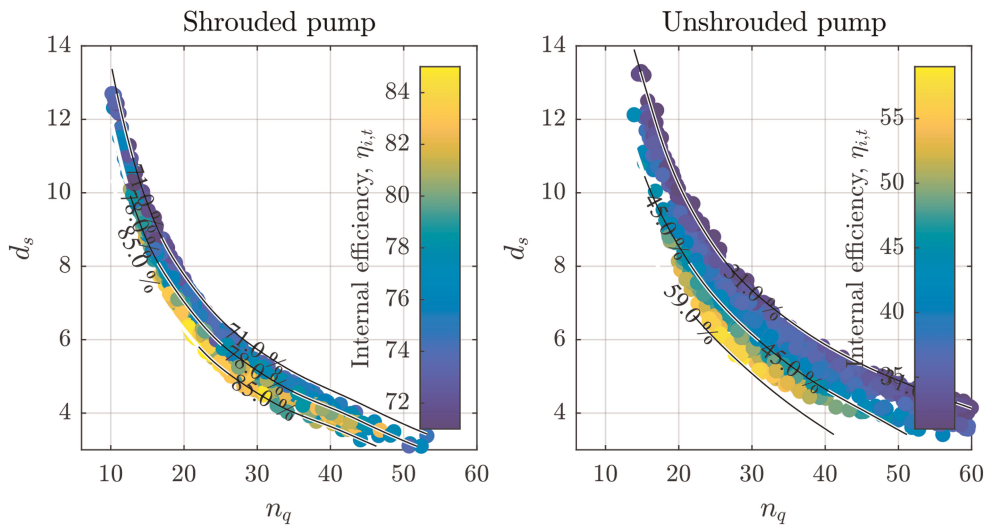


Figure 3. Efficiency distribution in the $n_q - d_s$ diagram for shrouded and unshrouded turbopumps.

Table 3. Pre-design correlations.

Geometry	Correlation	
Shrouded	$\eta_{i,t} = 227.7091 + 0.4423d_s^2 + 0.1043n_q^2 - 4.882n_q - 13.4851d_s - 0.1008n_qd_s - 0.0009n_q^3$	(15)
	$d_s = 9.8564e^{-0.0269n_q} + 20.1711e^{-0.1503n_q}$	(16)
Unshrouded	$\eta_{i,t} = 265.1359 + 0.7301d_s^2 + 0.0733n_q^2 - 0.037\frac{n_q^2}{d_s} - 5.5275n_q - 22.077d_s - 0.0003n_q^3$	(17)
	$d_s = 17.455e^{-0.0413n_q} + 8.8408e^{-0.1333n_q}$	(18)

The 1D modeling with neural networks

Zakeralhoseini and Schiffmann (2022a), (2023b) showed that the validity of current models for the effects of tip clearance is questionable for small-scale turbopumps and proposed neural network (NN)-based surrogate models to account for the influence of tip clearance and splitters on the slip factor and head loss coefficient of turbopumps. These models are trained on a wide range of design parameters using the CFD results, and are available in a data repository published by Zakeralhoseini and Schiffmann (2022b).

The slip factor model takes the tip clearance ratio, the number of blades, β_{2B} , and the flow coefficient as input parameters (see Equation 19). The head coefficient model takes β_1 , d_1/d_2 , and n_q in addition to the input parameters of the slip model (see Equation 20). When splitter blades are considered, the models will also need the splitters' pitch and relative meridional length. The slip factor model predicts the slip of both shrouded and unshrouded impellers. In contrast, the head coefficient model estimates the relative head loss of an unshrouded impeller compared to the same shrouded impeller.

$$\gamma = f(\beta_{2B}, Z, c/b, \phi, \varphi_{sp}, m'_{le,sp}) \tag{19}$$

$$\frac{\psi_{sh} - \psi_{unsh}}{\psi_{sh}} = f(n_q, \beta_{2B}, \beta_{1B}, d_1/d_2, Z, c/b, \phi, \varphi_{sp}, m'_{le,sp}) \tag{20}$$

Figure 4 presents an overview of how the new pre-design maps (0D models) and NN 1D models are linked for the design of centrifugal pumps. The process is started with the 0D model, which is based on principles of similarity. Figure 3 and (Equations 1 and 2) define relationships between specific numbers (n_q and d_s), head rise, and mass flow rate, guiding the determination of rotational speed (n) and impeller outlet diameter (d_2) based on specified requirements. These initial design values are then used as inputs for mean-line calculations to derive

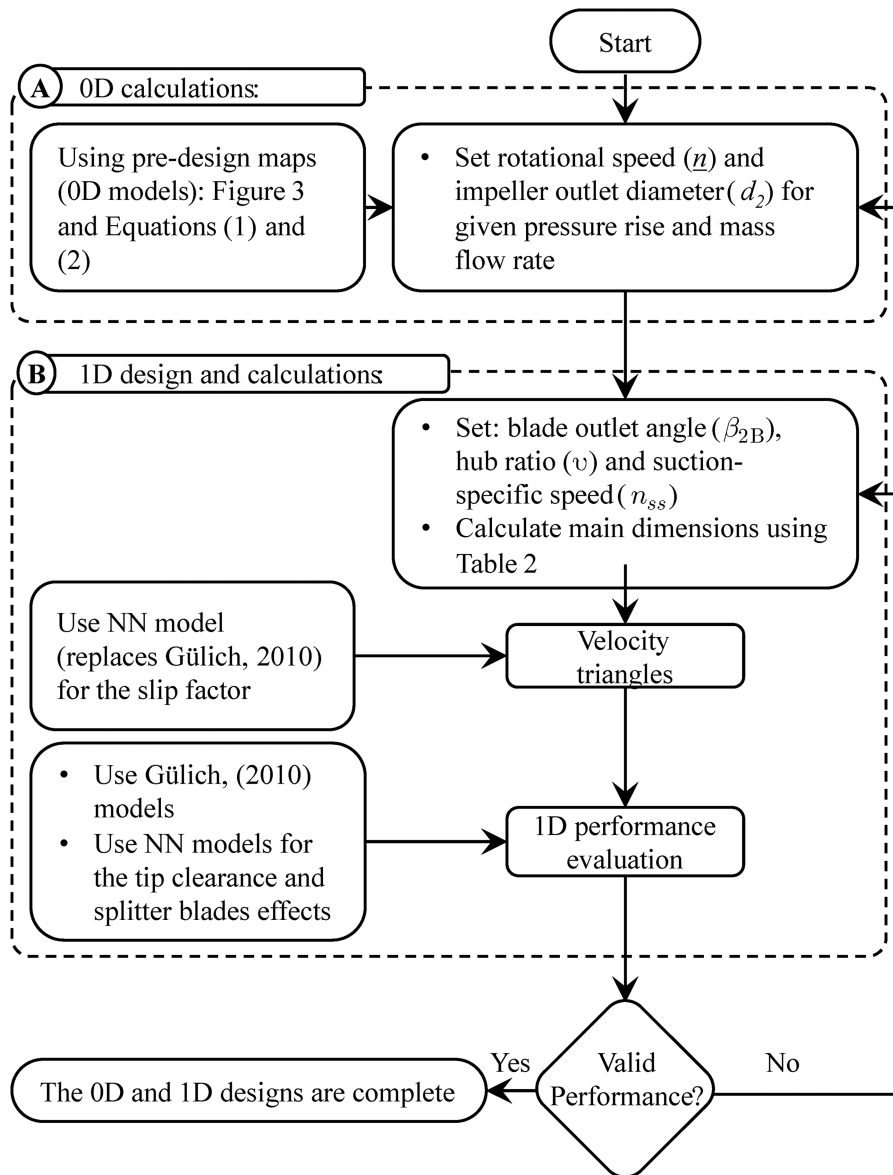


Figure 4. Diagram of 0D and 1D design processes.

geometrical parameters and velocity triangles at each station using equations provided in Table 2. The developed NN slip factor model replaces existing models (e.g., Gülich, 2010) to determine flow variables at the impeller outlet. Once geometrical parameters are established, the machine performance is assessed using the 1D model that incorporates empirical loss correlations (e.g., Gülich, 2010), including the tip clearance model proposed by Gülich (2010):

$$\frac{\psi_{sb} - \psi_{unsh}}{\psi_{sb}} = \frac{2.5(c/d_2)}{\sqrt{(b_2/d_2)(1 - (d_1/d_2))Z(e/t_2)^{0.2}n_q^{0.1}(\sin \beta_2)^{1.2}(\sin \beta_1)^{0.4}}} \quad (21)$$

The developed NN models for tip clearance effects (Zakeralhoseini and Schiffmann, 2022a) and splitter blades (Zakeralhoseini and Schiffmann, 2023b), are integrated into the 1D models to predict pump head rise and efficiency. The design process can be used to iterate and refine the turbopump geometry to achieve specified performance criteria for given inputs.

Experimental turbopumps and validation

Two turbopumps, sized for specific speeds of 8.9 and 28.5, are designed for experimental investigation using the same automated design tool and parameters detailed in Numerical procedure section. Two specific speeds are

chosen to assess the models across two distinct machines. The specifications (pressure rise and mass flow rate) of turbopump 2 are specifically designed to meet the pumping requirements of the ORC developed and tested by Rosset et al. (2021). The specifications of turbopump 1 are selected to test the models at different non-dimensional numbers. Table 4 presents the specifications and dimensions of experimental turbopumps working with R134a. Since performance characteristics are evaluated in non-dimensional forms, R134a is chosen over R245fa for experimental investigation due to its availability in the laboratory and lower cost. This does not impact the results, as the tests are conducted within the same range of non-dimensional numbers for R134a as for R245fa. The designed tip clearance is 100 μm for both turbopumps, corresponding to 7% and 8% of the blade outlet width for turbopump 1 and turbopump 2, respectively. Although updated pre-design maps are generated for a tip clearance ratio of 5%, corresponding to 61.75 μm and 72.1 μm , the experimental tip clearance is maintained at 100 μm to ensure accurate measurement and facilitate precise assembly. For turbopump 1, the blade outlet angle and number of blades are set to $\beta_{2B} = 27.5^\circ$ and 6, respectively, as recommended by Gülich (2010) to increase the efficiency of the machine. For turbopump 2, the blades are radially shaped ($\beta_{2B} = 90^\circ$) to increase the head rise for a given rotational speed and outlet diameter. Its impeller splitter blades, with a length equal to 55% of the main blades' length, positioned in the middle of the adjacent main blades (see Figure 5) to further enhance the pressure rise, as recommended by Zakeralhoseini and Schiffmann (2023b). The volute spiral is built with rectangular cross-sections, following Lobanoff and Ross (2013) recommendation for low specific speed pumps to prevent excessively large cross-sections.

Experimental analysis

The test rig represented in Figure 6 consists of a pump test section, an expansion valve, a condenser, a sub-cooler, and an evaporator (Zakeralhoseini and Schiffmann, 2023a). The pump test section (see Figure 7) consists of the turbopump, the spindle drive, mass flow meters, and the pressure and temperature sensors at the pump inlet and discharge. Instruments are connected to a data acquisition system governed by LabVIEW. The test conditions are controlled by heating and cooling loads applied to the heat exchangers. The rotor speed is controlled by the spindle drive control unit. The electric spindle drives the hermetic turbopump through a magnetic coupling. Preloaded ball bearings support the rotor and are lubricated directly with the working fluid.

Table 4. Main dimensions and operating conditions of the experimental turbopump.

Item	Parameter	Symbol	Unit	Turbopump 1	Turbopump 2
Experimental characteristics (post-calculated)	Specific speed	n_q	–	28.5	8.9
	Pressure rise at the design point	Δp	bar	$6.169 \pm 0.75\%$	$18.4 \pm 0.29\%$
	Mass flow rate	\dot{m}_r	kg s^{-1}	$0.140 \pm 0.15\%$	$0.280 \pm 0.15\%$
	Rotational speed	n	rpm	50,000	25,000
Impeller	Blade trailing edge angle	β_{2B}	$^\circ$	27.5	90
	Number of blades	Z	–	6	8
	Outlet diameter	d_2	mm	12.93	37.75
	Outlet width	b_2	mm	1.235	1.442
Volute	The base shape of cross-sections	–	–	Elliptic/Circular	Rectangular
	Cutwater diameter	d_{cw}	mm	13.62	42.0

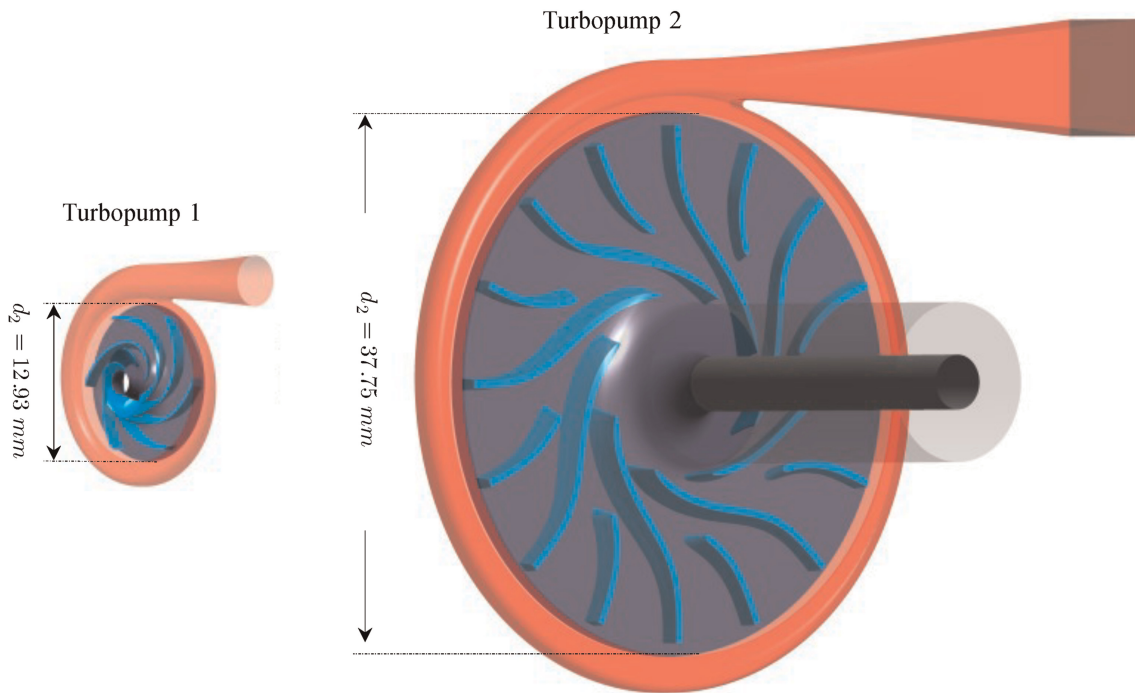


Figure 5. Turbopump 1 (left) and turbopump 2 (right).

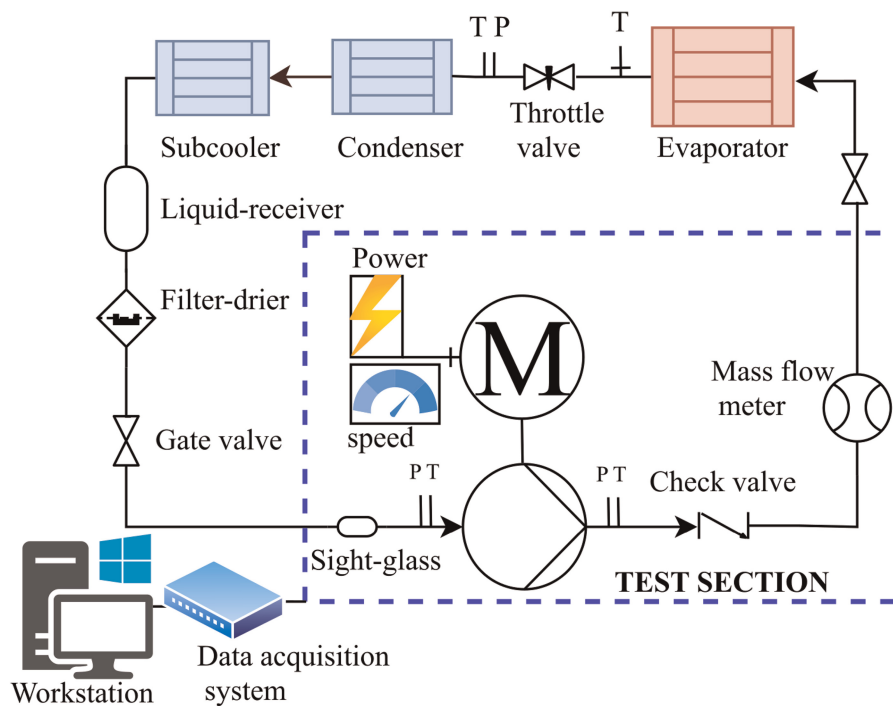


Figure 6. The flow diagram of the test rig.

Data reduction method

The LabVIEW interface utilizes REFPROP (Lemmon et al., 2018) to assess the working fluid thermodynamic properties and post-process sensor data, with post-processing relations summarized in Table 5.

Characteristic curves of experimental turbopumps

Figure 8 presents the experimental and CFD-based head rise and efficiency curves for the two turbopump designs operated at different rotational speeds. The CFD analysis and experimental results exhibit a maximum

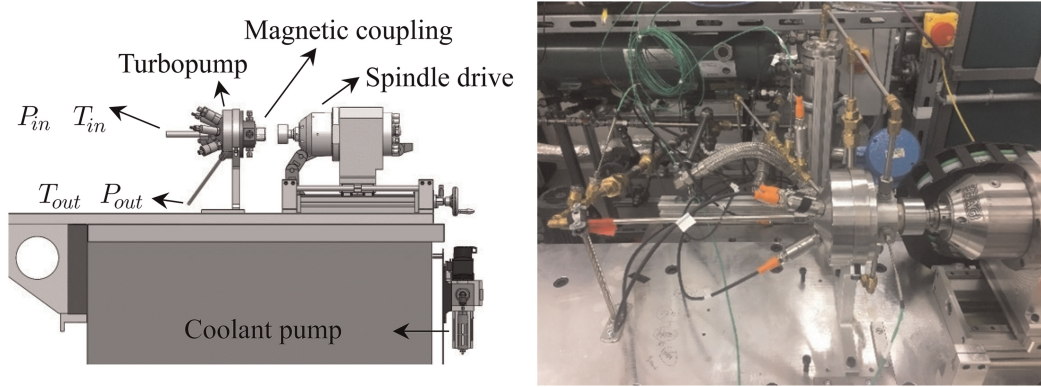


Figure 7. The test section.

Table 5. Post-processing equations of experimental data.

Parameter	Equation	
Useful power given to the flow	$\dot{W}_{us} = (\rho_o - \rho_{in})Q$	(22)
Total power given to the flow	$\dot{W}_t = \dot{m}(h_o - h_{in})$	(23)
Internal efficiency	$\eta_{i,t} = \dot{W}_{us}/\dot{W}_t$	(24)
Head coefficient	$\psi = gH/u_2^2$	(25)
Flow coefficient	$\phi = Q/r_2^2 u_2$	(26)
Back-work ratio	$BWR = \dot{W}_p/\dot{W}_T$	(27)
Thermal efficiency	$\eta_{th} = (\dot{W}_T - \dot{W}_p)/\dot{Q}_h$	(28)

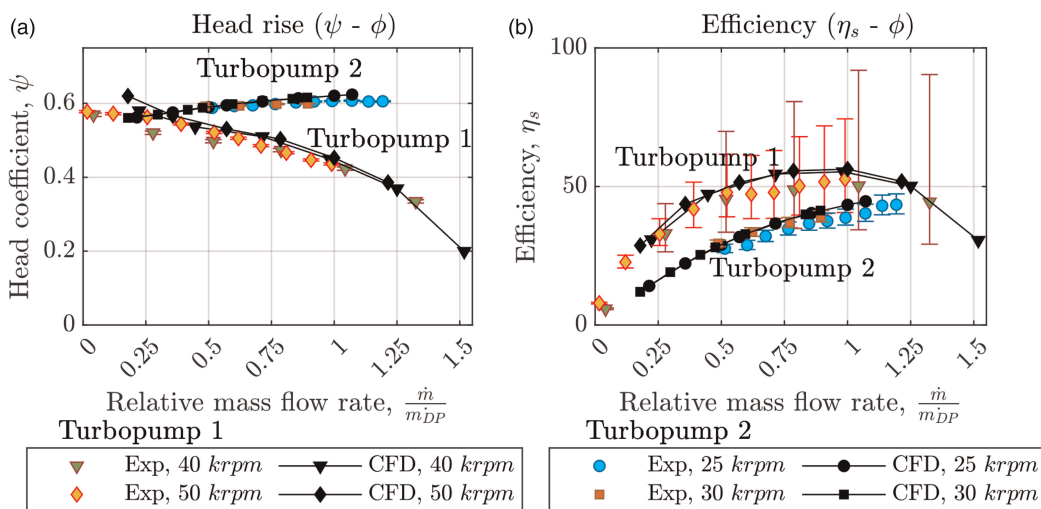


Figure 8. Experimental and CFD performance characteristics of turbopumps.

deviation of 3.51% for the head coefficient and 11.5% on the efficiency, demonstrating the high accuracy of the CFD modeling approach, which has been used to generate the data for inferring the pre-design maps and update the loss correlations. Turbopump 2 with a β_{2B} of 90° shows little variation in the head coefficient with capacity,

which agrees with the Euler equation. In contrast, turbopump 1 with a β_{2B} of 27.5° exhibits a significant decrease in head coefficient with increasing capacity. The figure also suggests that similarity laws apply to unshrouded pumps, as the results for different rotor speeds collapse onto the same head-capacity curves.

ORC performance characteristics

An existing ORC system designed for waste heat recovery from truck engines is used as a baseline to investigate the influence of the developed turbopumps on its performance. The system incorporates a small-scale, oil-free 8 kW radial inflow turbine supported on gas-lubricated bearings developed and tested by Rosset et al. (2021). Initially, the ORC system was driven by a 27-stage GRUNDFOS (CRNE 1–27) centrifugal pump with a maximum rotational speed of 3,000 rpm to achieve the required pressures. Excluding its drive, this commercial pump has a height of 716 mm and a volume of 51 L. In contrast, the tested small-scale turbopumps occupy only 3% of the commercial pump volume. Figure 9 compares the performance of the ORC system using the small-scale turbopumps with the original multi-stage centrifugal pump. The results suggest that the back-work ratio (BWR, see Equation 27) decreases up to 11.6 points and 6.8% points of the generator output power and is 67 and 42% lower for turbopumps 1 and 2, respectively, compared to the commercial pump. Moreover, the figure suggests that in addition to offering a much more compact solution (factor 33), using small-scale turbopumps can lead to a mean increase of 0.51% points in thermal efficiency.

Application of proposed models in the design of ORC turbopumps

The accuracy of the developed 0D and 1D models in predicting the impeller diameter is assessed and compared with state-of-the-art models. Using a reverse approach, the models are employed to estimate the impeller diameter necessary to achieve the experimental pressure rise at design flow rate as summarized in Table 4. Equation 2 can be reformulated as (Equation 29) to estimate the impeller outlet diameter:

$$d_{2,i} = f_i \frac{d_s Q^{1/2}}{(gH)^{1/4}} \quad (29)$$

The initial impeller diameter is estimated through the utilization of the pre-design map, which offers an initial guess to start the design process (square symbol in Figure 10). Subsequently, the impeller diameter is modified through an iterative process using the 1D-model (black circle symbol in Figure 10) while maintaining a constant blade outlet angle to achieve the required pressure rise. To correct the impeller outlet diameter, the factor f_i is introduced in (Equation 29) to adjust the impeller outlet diameter based on estimations derived from 1D models. The iterative process begins with $f_0 = 1$. For each iteration step, the pump head rise is estimated using the methodology described in Figure 4. Subsequently, the impeller outlet diameter is adjusted in accordance with (Equation 30):

$$f_i = f_{i-1} - \frac{H_i - H}{H_i} \quad (30)$$

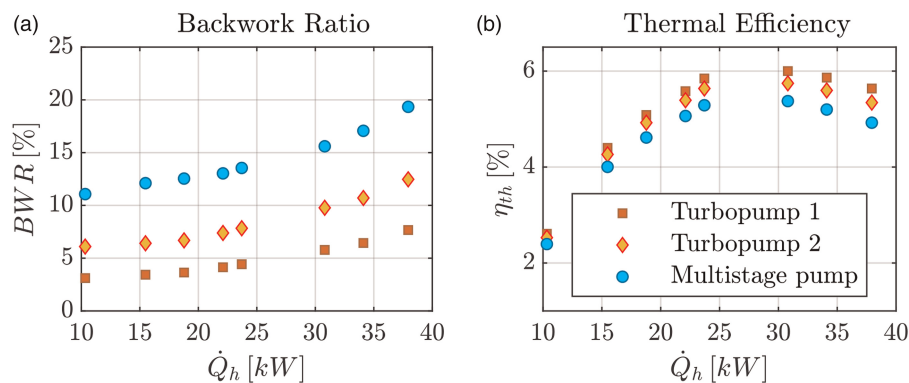


Figure 9. Comparison of performance characteristics for the targeted ORC system.

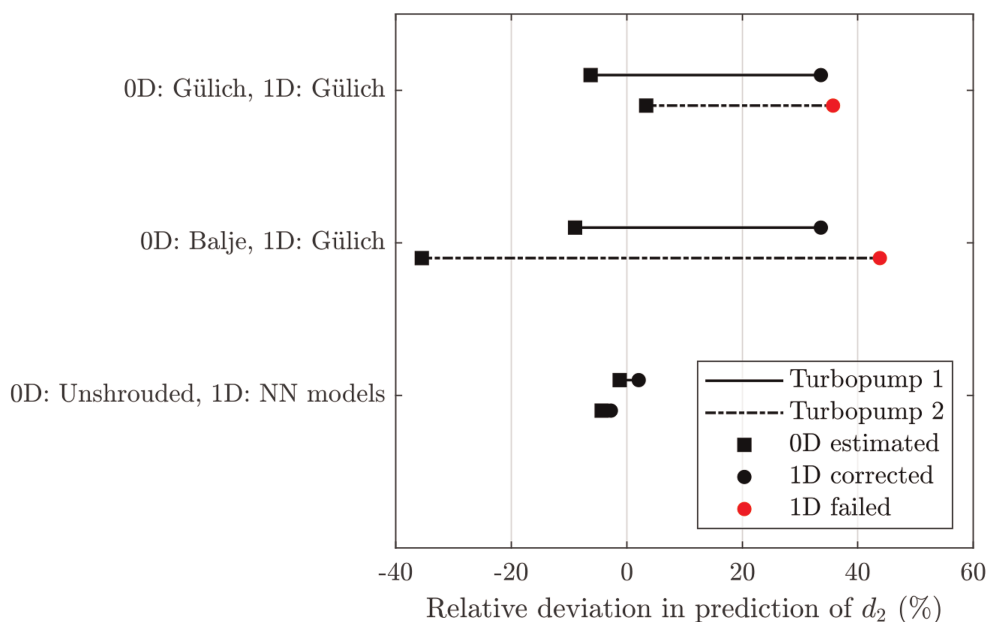


Figure 10. Deviation of d_2 predicted with correlations from experimental turbopumps.

where, H represents the specified head rise and H_i the estimated head rise in the i^{th} iteration. The iterations continue until the estimated head rise converges to the head rise requirement with a tolerance of 10^{-3} for the relative head rise, as per (Equation 31):

$$\varepsilon = \left| \frac{H_i - H}{H} \right| \quad (31)$$

Figure 10 summarizes the estimated diameter deviations relative to the ones of the tested impellers, using state-of-the-art models and the ones introduced in this work. The square symbols represent the tip diameter estimated with Gülich (2010), Balje (1962), and the updated pre-design maps for shrouded and unshrouded designs. The circle symbols represent the impeller diameter obtained by applying correlations by Gülich (2010) and the updated 1D-models using the initial guess originating from the pre-design maps. The combinations of the used pre-design maps and the 1D-model are highlighted by the double label along the y-axis.

The comparison in Figure 10 suggests that, for both turbopumps, the unshrouded pre-design map presented in this work provides the most accurate estimate of the impeller diameter, followed by the Gülich (2010) model (Equation 3). The Balje (1981) diagram underpredicts the impeller diameter by 8.9% for turbopump 1, and by 35.5% for turbopump 2. When using the NN-based 1D-models (Zakeralhoseini and Schiffmann, 2022a, 2023b) for slip factor and tip clearance to correct the impeller diameter, the estimation deviation is only 3%. However, when using the models from Gülich (2010) for turbopump 1, the deviation is around 33.7%. For turbopump 2 (red circle symbol), the correction of impeller diameter does not converge when using the models from Gülich (2010) due to inaccuracies in predicting tip clearance losses, as discussed by Zakeralhoseini and Schiffmann (2022a), leading to negative head rise estimations.

Utilizing the models developed in this study is suggested to significantly reduce the design time of a turbopump, due to the much more accurate initial prediction of the impeller diameter. The impeller diameter necessary to meet the required pressure rise can be attained through a mere two iterations with the updated pre-design maps and 1D-model. In contrast, the Gülich (2010) models exhibit an initial impeller diameter deviation of over 33% and fail to converge for turbopump 2, which suggests that the latter is not feasible. Such imprecise estimation introduces substantial bias to the design and extends the number of design iterations in the CFD analysis stage. Notably, each CFD iteration takes a significant amount of time on today's powerful computers, whereas the 1D calculations are executed almost instantaneously, highlighting the benefit of the updated pre-design maps and improved 1D models.

Conclusions

Small-scale single-stage turbopumps offer cost reduction in materials, simplified mechanical design, space efficiency, and fuel savings for driving ORC systems. To ensure that a turbopump is efficient and reliable and meets

the specifications for its application, an iterative process is needed, which starts with simple pre-design maps and iteratively moves to 1D-meanline models and ends with 3D-CFD simulations to continuously refine the geometry. State-of-the-art models have been shown to fail for the design of turbopumps suited for small-scale ORC.

To address this shortcoming, a parameterized design model that allows for the automated design and CFD evaluation of turbopump geometries is developed to characterize the performance of numerous turbopump geometries for small-scale ORC applications. Based on this post-processed CFD-data, pre-design maps and 1D models, which have proven to be effective tools for designing pumps, are developed for small-scale ORC applications. The presented models can reduce the time and cost associated with the iterative design process.

The models' validity is verified through experiments on small-scale turbopumps. The very small deviations observed between the CFD analyses and experimental results validate the numerical approach conducted on the small-scale turbopumps for ORC systems. Compared to a 27-stage commercial turbopump, the small-scale single stage turbopumps presented in this work are expected to improve the thermal efficiency of the ORC by 0.51% and decrease the BWR by up to 67%.

This study represents a significant step in developing compact and efficient turbopumps for ORC systems, which opens exciting avenues for future research. The updated n_q-d_s diagrams and the new 1D models obtained through data-driven approaches are validated against two experimental turbopumps with specific speeds of 8.9 and 28.5. Further experimental investigations are needed to explore additional small-scale turbopumps with different geometric features, to extend the validation of the pre-design maps at various specific speeds.

Nomenclature

b	channel width, m
c	tip clearance, m
\bar{c}	absolute velocity, m s^{-1}
d	diameter, m
d_s	specific diameter
e	blade thickness, m
g	gravity, m s^{-2}
H	head, m
h	enthalpy, J
m	meridional length, m
\dot{m}	mass flow rates, kg s^{-1}
n	rotational speed, rpm
n_q	specific speed
n_{ss}	suction specific speed
p	total pressure, Pa
Q	flow rate, $\text{m}^3 \text{s}^{-1}$
\dot{Q}	heat transfer rate, W
t	blade blockage factor
u	peripheral velocity, m s^{-1}
Z	number of blades
\bar{w}	relative velocity, m s^{-1}
\dot{W}	power, W

Greek letters

α	absolute flow angle, $^\circ$
β_B	blade angle, $^\circ$
β	flow angle, $^\circ$
η	efficiency
ρ	density, kg m^{-3}
v	hub ratio
γ	slip factor
φ_{sp}	pitch of splitters
ϕ	flow coefficient
ψ	head coefficient

Subscripts

<i>cw</i>	cutwater
<i>DP</i>	design point
<i>i</i>	internal
<i>in</i>	inlet
<i>EV</i>	Evaporator
<i>h</i>	hub
<i>mb</i>	main blade
<i>le</i>	leading edge
<i>o</i>	outlet
<i>P</i>	pump
<i>s</i>	shroud
<i>sh</i>	shrouded
<i>T</i>	turbine
<i>th</i>	thermal
<i>sp</i>	splitter blades
<i>t</i>	total
<i>unsh</i>	unshrouded
<i>us</i>	useful
<i>1</i>	impeller inlet
<i>2</i>	impeller outlet

Abbreviations

BWR	back-work ratio
CFD	computational fluid dynamics
ORC	organic Rankine cycle
1D	one dimensional
3D	three dimensional

Competing interests

Sajjad Zakeralhoseini declares that he has no conflict of interest. Jürg Schiffmann declares that he has no conflict of interest.

References

-
- Ansys* (Release 2021 R1). (2021). ANSYS Inc.
- Balje O. E. (1962). A study on design criteria and matching of turbomachines: Part B—compressor and pump performance and matching of turbocomponents. *Journal of Engineering for Power*. 84 (1): 103–114. <https://doi.org/10.1115/1.3673350>.
- Balje O. E. (1981). *Turbomachines—A Guide to Design, Selection, and Theory* (Issue BOOK). New York: John Wiley & Sons.
- Bao J., and Zhao L. (2013). A review of working fluid and expander selections for organic Rankine cycle. *Renewable and Sustainable Energy Reviews*. 24: 325–342. <https://doi.org/10.1016/j.rser.2013.03.040>.
- Benato A. and Macor A. (2017). Biogas engine waste heat recovery using organic Rankine cycle. *Energies*. 10 (3): 327.
- Bianchi G., Fatigati F., Murgia S., and Cipollone R. (2017). Design and analysis of a sliding vane pump for waste heat to power conversion systems using organic fluids. *Applied Thermal Engineering*. 124: 1038–1048. <https://doi.org/10.1016/j.applthermaleng.2017.06.083>.
- Diehl M., Schreiber C., and Schiffmann J. (2020). The role of Reynolds number effect and tip leakage in compressor geometry scaling at low turbulent Reynolds numbers. *Journal of Turbomachinery*. 142 (3): 031003. <https://doi.org/10.1115/1.4045465>.
- Freyman R., Strobl W., and Obieglo A. (2008). The turbosteamer: A system introducing the principle of cogeneration in automotive applications. *MTZ Worldwide*. 69: 20–27. <https://doi.org/10.1007/BF03226909>.
- Galindo J., Ruiz S., Dolz V., Royo-Pascual L., Haller R., et al. (2015). Experimental and thermodynamic analysis of a bottoming organic Rankine Cycle (ORC) of gasoline engine using swash-plate expander. *Energy Conversion and Management*. 103: 519–532. <https://doi.org/10.1016/j.enconman.2015.06.085>.
- Gulich J. (2010). *Centrifugal pumps*. Berlin Heidelberg: Springer.
- Ibaraki S., Endo T., Kojim Y., Takahashi K., Baba T., and Kawajiri S. (2007). Study of efficient on-board waste heat recovery system using rankine cycle. *Review of Automotive Engineering*. 28 (3): 307–313.
- Japikse D., Marscher W., and Furst R. (2006). *Centrifugal Pump Design and Performance*. White River Junction, Vermont: Concepts NREC.
- Landelle A., Tauveron N., Revellin R., Haberschill P., Colasson S., and Roussel V. (2017). Performance investigation of reciprocating pump running with organic fluid for organic Rankine cycle. *Applied Thermal Engineering*. 113: 962–969. <https://doi.org/10.1016/j.applthermaleng.2016.11.096>.

- Lecompte S., Huisseune H., Van Den Broek M., Vanslambrouck B., and De Paepe M. (2015). Review of organic Rankine cycle (ORC) architectures for waste heat recovery. *Renewable and Sustainable Energy Reviews*. 47: 448–461.
- Lei B., Wang J. F., Wu Y. T., Ma C. F., Wang W., et al. (2016). Experimental study and theoretical analysis of a Roto-Jet pump in small scale organic Rankine cycles. *Energy Conversion and Management*. 111: 198–204. <https://doi.org/10.1016/j.enconman.2015.12.062>.
- Lemmon E. W., Bell I. H., Huber M. L., and McLinden M. O. (2018). NIST standard reference database 23: Reference fluid thermodynamic and transport properties-REFPROP, version 10.0. In National Institute of Standards and Technology. Standard Reference Data Program, Gaithersburg.
- Lobanoff V. S. and Ross R. R. (2013). *Centrifugal Pumps: Design and Application*. Houston: Elsevier.
- Meng F., Zhang H., Yang F., Hou X., Lei B., et al. (2017). Study of efficiency of a multistage centrifugal pump used in engine waste heat recovery application. *Applied Thermal Engineering*. 110: 779–786. <https://doi.org/10.1016/j.applthermaleng.2016.08.226>.
- Menter F., Kuntz M., and Langtry R. B. (2003). Ten years of industrial experience with the SST turbulence model. *Heat and Mass Transfer*. 4: 625–632.
- Nelson C. R. (2006). Heavy duty truck engine – achieving high engine efficiency at 2010 emissions. In *Cummins, DEER Conference*.
- Nourbakhsh S. A. (2005). *Turbomachinery*: Tehran: University of Tehran Press.
- Olimstad G., Osvoll M., and Finstad P. H. E. (2018). Very low specific speed centrifugal pump—hydraulic design and physical limitations. *Journal of Fluids Engineering*. 140 (7): 071403. <https://doi.org/10.1115/1.4039250>.
- Pfeiderer C. (2013). *Die Kreiselpumpen für Flüssigkeiten und Gase: Wasserpumpen, Ventilatoren, Turbogebläse Turbokompressoren*. Berlin: Springer-Verlag.
- Rijpkema J., Munch K., and Andersson S. B. (2017). Thermodynamic potential of Rankine and flash cycles for waste heat recovery in a heavy duty Diesel engine. *Energy Procedia*. 129: 746–753. <https://doi.org/10.1016/j.egypro.2017.09.110>.
- Ringler J., Seifert M., Guyotot V., and Hübner W. (2009). Rankine cycle for waste heat recovery of IC engines. *SAE International Journal of Engines*. 2 (1): 67–76. <https://doi.org/10.4271/2009-01-0174>.
- Rosset K., Pajot O., and Schiffmann J. (2021). Experimental investigation of a small-scale organic Rankine cycle turbo-generator supported on gas-lubricated bearings. *Journal of Engineering for Gas Turbines and Power*. 143 (5): 1–14. 51015. <https://doi.org/10.1115/1.4049988>.
- Stepanoff A. (1957). *Centrifugal and Axial Flow Pumps: Theory, Design, and Application*. New York: Wiley.
- von Backström T. W. (2005). A unified correlation for slip factor in centrifugal impellers. *Journal of Turbomachinery*. 128 (1): 1–10. <https://doi.org/10.1115/1.2101853>.
- Wang J., Yan Z., Wang M., Ma S., and Dai Y. (2013a). Thermodynamic analysis and optimization of an (organic Rankine cycle) ORC using low grade heat source. *Energy*. 49: 356–365. <https://doi.org/10.1016/j.energy.2012.11.009>.
- Wang T., Zhang Y., Zhang J., Shu G., and Peng Z. (2013b). Analysis of recoverable exhaust energy from a light-duty gasoline engine. *Applied Thermal Engineering*. 53 (2): 414–419. <https://doi.org/10.1016/j.applthermaleng.2012.03.025>.
- Xu W., Zhang J., Zhao L., Deng S., and Zhang Y. (2017). Novel experimental research on the compression process in organic Rankine cycle (ORC). *Energy Conversion and Management*. 137: 1–11. <https://doi.org/10.1016/j.enconman.2017.01.025>.
- Xu B., Rathod D., Yebi A., Filipi Z., Onori S., and Hoffman M. (2019). A comprehensive review of organic rankine cycle waste heat recovery systems in heavy-duty diesel engine applications. *Renewable and Sustainable Energy Reviews*. 107: 145–170. <https://doi.org/10.1016/j.rser.2019.03.012>.
- Yamamoto T., Furuhashi T., Arai N., and Mori K. (2001). Design and testing of the organic Rankine cycle. *Energy*. 26 (3): 239–251. [https://doi.org/10.1016/S0360-5442\(00\)00063-3](https://doi.org/10.1016/S0360-5442(00)00063-3).
- Yang Y., Zhang H., Xu Y., Yang F., Wu Y., and Lei B. (2018a). Matching and operating characteristics of working fluid pumps with organic Rankine cycle system. *Applied Thermal Engineering*. 142: 622–631. <https://doi.org/10.1016/j.applthermaleng.2018.07.039>.
- Yang Y., Zhang H., Xu Y., Zhao R., Hou X., and Liu Y. (2018b). Experimental study and performance analysis of a hydraulic diaphragm metering pump used in organic Rankine cycle system. *Applied Thermal Engineering*. 132: 605–612. <https://doi.org/10.1016/j.applthermaleng.2018.01.001>.
- Yang Y., Zhang H., Tian G., Xu Y., Wang C., and Gao J. (2019). Performance Analysis of a Multistage Centrifugal Pump Used in an organic Rankine Cycle (ORC) System under Various Condensation Conditions. *Journal of Thermal Science*. 28 (4): 621–634. <https://doi.org/10.1007/s11630-019-1069-9>.
- Zakeralhoseini S. and Schiffmann J. A. (2021). The effects of the tip clearance on the performance of small-scale turbopumps for ORC applications; analysis and modeling. In *Proceedings of the 6th International Seminar on ORC Power Systems*, Vol. 2021 (112).
- Zakeralhoseini S. and Schiffmann J. (2022a). Analysis and modeling of the tip leakage flow on the performance of small-scale turbopumps for ORC applications. *Applied Thermal Engineering*. 217: 119160. <https://doi.org/10.1016/j.applthermaleng.2022.119160>.
- Zakeralhoseini S. and Schiffmann J. (2022b). *Neural Network Models for Centrifugal Pumps (No. 2): Mendely Data*. Amsterdam, Netherlands: Elsevier.
- Zakeralhoseini S., and Schiffmann J. (2023a). Design, computational and experimental investigation of a small-scale turbopump for organic Rankine cycle systems. *Energy Conversion and Management*. 287: 117073. <https://doi.org/10.1016/j.enconman.2023.117073>.
- Zakeralhoseini S., and Schiffmann J. (2023b). The influence of splitter blades and meridional profiles on the performance of small-scale turbopumps for ORC applications; analysis, neural network modeling and optimization. *Thermal Science and Engineering Progress*. 39: 101734. <https://doi.org/10.1016/j.tsep.2023.101734>.
- Zakeralhoseini S. and Schiffmann J. (2024). Small-scale turbopumps for waste heat recovery applications based on an organic Rankine cycle, modeling, analytical and experimental investigations. In *Proceedings of the 7th International Seminar on ORC Power System*, pp. 655–664.